applied sciences

MDPI

Article

The Gas Migration During the Drainage Process of Ultra-Long Directional Boreholes in Coal Seams

Shuaiyin He [1], Mingyao Wei [2,*] and Yingke Liu [3]

[1] CHN Shendong Coal Group Co., Ltd., Shenmu 719315, China; shuaiyinhe@126.com
[2] National and Local Joint Engineering Laboratory of Internet Application Technology on Mine, IoT Perception Mine Research Center, China University of Mining and Technology, Xuzhou 221116, China
[3] School of Safety Engineering, China University of Mining and Technology, Xuzhou 221116, China; ykliu@cumt.edu.cn
* Correspondence: cumtwmy@sina.com

Abstract

The use of ultra-long directional drilling holes for large-scale pre-drainage of gas in coal seams offers advantages such as extensive coverage and high efficiency, but its effectiveness in deep coal seams remains unclear. Focusing on the seepage characteristics of the No. 8 coal seam in the Baode Mining Area of Shanxi Province, experimental tests were conducted to investigate the evolution of dual-scale porosity permeability. The relationship between matrix/fracture permeability and effective stress were built. Utilizing numerical simulations, this study reveals the nonlinear mechanism in which permeability behavior during gas drainage is jointly influenced by pore pressure reduction and matrix shrinkage. Field measurements and simulation results demonstrated that in shallow borehole regions (<1500 m), permeability increased by up to 3.5 times, while in deeper regions (>2000 m), drainage efficiency significantly declined due to limited pressure drop propagation. These findings provide theoretical support for optimizing the layout of ultra-long directional drilling holes, enhancing gas drainage efficiency, and ensuring safe mining operations.

Keywords: safety science and engineering; dual-scale porosity; permeability evolution; gas drainage; gas-solid coupling; numerical simulation

check for updates

Academic Editor: Ricardo Castedo

Received: 29 August 2025
Revised: 23 September 2025
Accepted: 24 September 2025
Published: 25 September 2025

Citation: He, S.; Wei, M.; Liu, Y. The Gas Migration During the Drainage Process of Ultra-Long Directional Boreholes in Coal Seams. *Appl. Sci.* **2025**, *15*, 10420. https://doi.org/10.3390/app151910420

Copyright: © 2025 by the authors. Licensee MDPI, Basel, Switzerland. This article is an open access article distributed under the terms and conditions of the Creative Commons Attribution (CC BY) license (https://creativecommons.org/licenses/by/4.0/).

1. Introduction

China possesses the world's largest coalbed methane (CBM) resources, with proven reserves exceeding 36.8 trillion cubic meters of unconventional natural gas [1]. As mining operations extend to greater depths, the in situ stress and pore pressure gradients in coal reservoirs increase. Accompanied by matrix shrinkage, swelling, and dynamic fracture evolution, these factors cause a nonlinear evolution in coal permeability. Permeability is a fundamental parameter describing the fluid transport capacity of multi-scale porous media. Understanding the evolution of permeability and its controlling mechanisms during CBM drainage is therefore critical for improving extraction efficiency and guiding engineering practice.

Coal is inherently a dual-porosity medium, comprising nanoscale matrix pores and a microscopic fracture network. This hierarchical pore–fracture system governs gas occurrence and migration through coupled adsorption–desorption and seepage processes [2]. Permeability is influenced by numerous factors, including: in situ stress conditions, reservoir temperature, pore pressure, and the physical characteristics of the permeating gas [3–5]. Due to the dual-porosity nature of coal, the permeability of the matrix and fractures evolves

differently during drainage [6]. Although fracture permeability is typically several orders of magnitude greater than that of the matrix, gas flow within the matrix can significantly influence CBM recovery rates [7].

Extensive studies have examined the mechanisms driving permeability evolution at different pore scales. They conducted an experimental study on permeability, investigating factors such as effective stress, pore pressure, gas adsorption/desorption, pore–fracture structural characteristics, and gas slippage. Wang et al. [8] conducted experimental studies on coal deformation and structural evolution under gas migration, reporting a nonlinear relationship between permeability and pore pressure. Li et al. [9], using nitrogen as the permeating gas, found that coal permeability varies exponentially with pore pressure. Lu et al. [10] systematically investigated the response of coal permeability to pore pressure and stress, establishing quantitative relationships and demonstrating that, under low gas pressure conditions, permeability decreases with increasing pore pressure following a power-law trend. Long [11] reported that permeability decreases with rising pore pressure due to both slippage effects and intrinsic changes in pore structure. Tang et al. [12] demonstrated a negative exponential relationship between permeability and pore pressure, attributable to the interaction between CBM desorption and seepage. Peng et al. [13] investigated the effect of matrix shrinkage and gas slippage on permeability under different gas conditions, while Zhu et al. [14] examined gas-bearing coal permeability under various stress paths, elucidating its relationships with axial stress, confining stress, and gas pressure, and establishing corresponding qualitative and quantitative models. Also, there have been a number of simulation scenarios used to investigate the methane flow rules based on a fully coupled numerical model with coal mass deformation, anisotropic gas flow in fractures, and anisotropic absorption/adsorption [15–18].

The coupled interaction between the matrix and fractures produces complex permeability evolution behaviors. While matrix permeability is often neglected in theoretical models due to its significantly lower magnitude compared with fracture permeability, multiphase flow and gas slippage within matrix micropores can markedly influence the overall permeability of the coal seam [19]. This, in turn, affects mining performance and CBM drainage efficiency. However, the permeability variation patterns of the matrix and fracture systems during coal seam gas extraction have not yet been clearly determined.

The present study combines experimental testing and theoretical modeling to determine the relationships between matrix and fracture permeability and effective stress. Using these results, numerical simulations are performed to investigate fracture permeability evolution during long directional borehole drainage under multiple influencing factors. The analysis further illustrates gas migration behavior in ultra-long boreholes, clarifies the effects of borehole depth on coal seam permeability and gas content. The study results provide a theoretical basis and optimization strategies for large-scale, pre-drainage CBM control.

2. Experimental Testing of Dual-Scale Permeability in Coal

The specimens used in this study were obtained from the No. 8 coal seam of the Baode mining area, Xinzhou City, Shanxi Province. The mining elevation of the No. 8 seam ranges from +940 m to +420 m, with a burial depth of 5~663 m. The seam has an average dip angle of 3.5°, an average pure coal thickness of 6.83 m, and is classified as a thick to extra-thick seam. The coal type is primarily gas coal, followed by long-flame coal, weakly caking coal, and 1/2 medium-caking coal.

Standard cylindrical specimens with a diameter of 50 mm and a length of 100 mm were prepared using a core drilling machine, oriented perpendicular to the bedding of the coal. The processed samples were dried at 60 °C for 24 h in a drying oven to remove internal moisture

and then sealed with plastic wrap for storage until testing. A coal–gas coupling test system was used for coal permeability measurements in this study [20]. Permeability experiments were conducted on coal samples under varying confining stress and pore pressure with constant temperature of 25 °C. The upstream gas pressure and downstream gas pressure were recorded during the measurement. The permeability of the sample can be calculated based on the pulse-decay method. Non-adsorptive helium was used as the test gas to minimize the effects of gas adsorption. Multiple seepage tests were conducted under various combinations of confining and pore pressures, corresponding to effective stress points of 2, 3, 4, 5, and 6 MPa. Detailed experimental conditions and equipment can be found in the literature [20].

The variation in total permeability with effective stress under different pore pressures is shown in Figure 1. Results indicate that, at a constant pore pressure, total gas-measured permeability decreases with increasing effective stress, exhibiting a negative exponential trend. Since non-adsorptive He was employed, the observed permeability variation can be attributed solely to stress, with adsorption-induced matrix swelling negligible. Based on the Klinkenberg slippage equation, a model was developed to calculate matrix permeability and fracture permeability separately [20]:

$$k_a = k_m\left(1 + \frac{16\mu}{\alpha r}\sqrt{\frac{\pi RT}{2M_g}}\frac{1}{p}\right) + \left(k_{pmax} - k_m\right) \quad (1)$$

where k_a is the measured gas permeability at average gas pressure (m^2); k_m is matrix permeability (m^2); r is the effective pore radius of the coal matrix (m); α is an empirical coefficient; μ is gas dynamic viscosity (Pa·s); T is temperature (K); R is the universal gas constant J/(mol·K); M_g is gas molecular mass (kg/mol); p is gas pressure during testing (Pa); and k_{pmax} is the permeability at high gas pressure when slippage effects are negligible (m^2). Using this model, the relationship between matrix, fracture permeability, and effective stress was estimated from the experimental data [20], as displayed in Figure 2. Low-field NMR measurements were also then conducted to obtain the T_2 distribution. The T_2 cutoff method was applied to partition the spectrum and quantify the respective volumes of the matrix and fracture pore systems. The pore size distribution of the coal samples was determined. The NMR T_2 distribution reveals a bimodal pore structure, with a pronounced peak below 1 ms corresponding to the microporous matrix and a broader peak centered around 20 ms, indicative of a well-developed fracture network. The low stress-sensitivity of permeability can be attributed to the pore structure characterized by NMR, which showed a significant proportion of the pore volume residing in large fractures and macropores. It reduces the stress sensitivity of permeability, making it less susceptible to compaction.

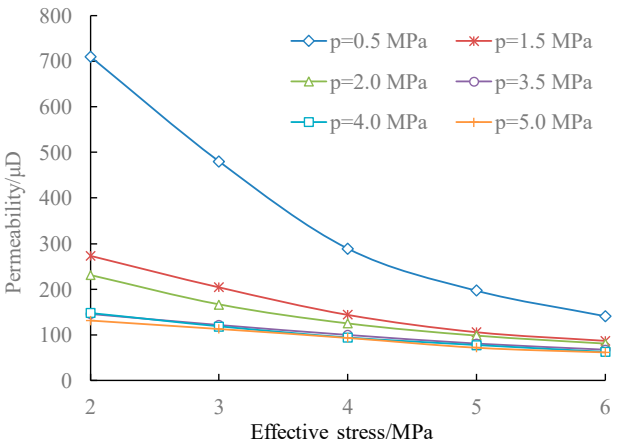

Figure 1. Relationship between coal permeability and effective stress under different pore pressures.

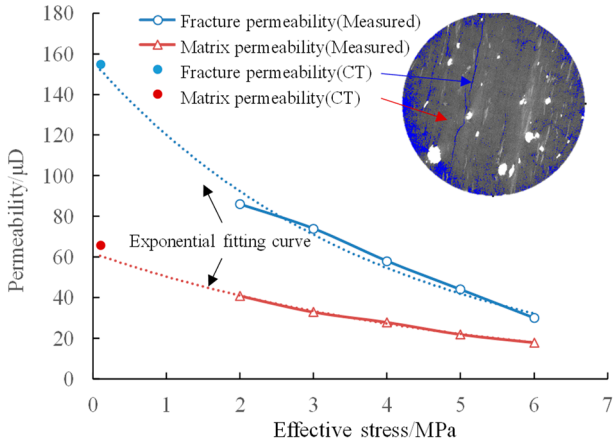

(**a**) Permeability vs. effective stresses

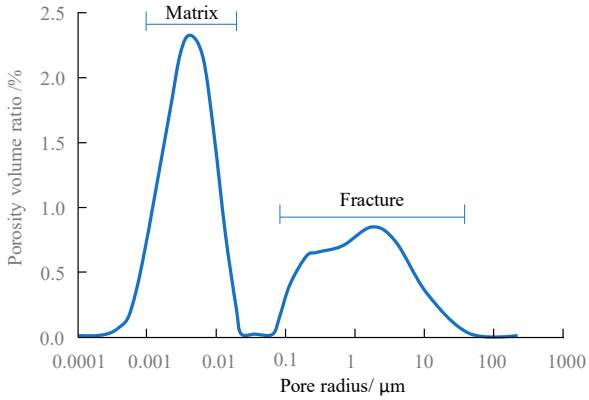

(**b**) Diameter distribution curve

Figure 2. Variation in coal matrix and fracture permeability under different effective stresses and its comparison with CT test results.

High-resolution CT scanning was conducted under unloaded conditions to characterize fracture and pore structures, and connectivity analysis was employed to quantify matrix and fracture permeability. Permeability values obtained from CT analysis displayed high consistency with those from the model-derived, both exhibiting an exponential dependence on effective stress, thereby validating the accuracy and reliability of the proposed model. Furthermore, the results suggest that the difference between matrix and fracture permeability is negligible. This phenomenon is attributed to its low metamorphic rank and the presence of large pore sizes. It causes that matrix permeability approaches that of the fractures. It shows that both matrix and fracture permeability decrease with increasing effective stress. The experimentally derived permeability–stress relationship provides essential input parameters for numerical simulations and modeling of coal permeability evolution.

3. Theoretical Model of Coal Seam Gas Seepage

3.1. Gas Flow Equation in the Matrix System

In the matrix system, the permeability of the matrix pores is greater than the intrinsic diffusivity of the matrix itself. The dual-porosity structure can more accurately represent the inherent structure of the matrix. Assuming that coal seam gas flow follows Darcy's law, the gas mass balance equation in coal reservoirs, according to the law of mass conservation, can be expressed as [21]:

$$\frac{\partial m}{\partial t} + \nabla \cdot (\rho_g u_g) = Q_s \tag{2}$$

where m is the mass of gas per unit volume of coal, including both free gas and adsorbed gas (kg); ρ_g is the gas density in the coal reservoir (kg/m^3); u_g is the Darcy velocity vector (m/s); Q_s is the gas source term (kg/(m^3·s)); and t is time (s). When gas adsorption is assumed to occur only in the coal matrix blocks, the gas mass per unit volume in the matrix and in the fractures can be mathematically expressed as [21]:

$$m_m = \rho_g \phi_m + (1 - \phi_m)\rho_{ga}\rho_s \frac{V_L p_m}{p_m + P_L} \tag{3}$$

$$m_f = \rho_g \phi_f \tag{4}$$

where the subscripts m, f, g, and s denote matrix, fracture, gas, and coal, respectively; ϕ is porosity; ρ_{ga} is the gas density at standard conditions (kg/m^3); V_L is the Langmuir volume constant (m^3/kg); P_L is the Langmuir pressure constant (Pa); and p_m is the gas pressure in the matrix (Pa). Based on the above equations, the governing equations for gas flow in the matrix and fracture systems of a dual-porosity medium can be derived [22]:

$$\left[\phi_m + (1 - \phi_m)\rho_{ga}\rho_s \frac{V_L p_m}{p_m + P_L}\right]\frac{\partial p}{\partial t} + p_m \frac{\partial \phi_m}{\partial t} + \nabla \cdot \left(-\frac{k_m}{\mu} p_m \nabla p_m\right) = \omega(p_m - p_f) \tag{5}$$

$$\phi_f \frac{\partial p_f}{\partial t} + p_f \frac{\partial \phi_f}{\partial t} + \nabla \cdot \left(-\frac{k_f}{\mu} p_f \nabla p_f\right) = -\omega(p_m - p_f) \tag{6}$$

where ω is the gas mass exchange coefficient between the matrix and fracture systems, which can be defined as:

$$\omega = \xi \frac{D}{\mu} \tag{7}$$

where ξ is the shape factor (typically taken as 2.5), and D is the diffusion coefficient in matrix micropores (m^2/s). Considering both the effects of matrix desorption-induced shrinkage and fracture gas pressure variation, the evolution equation for fracture permeability during gas extraction can be expressed as [23–28]:

$$\frac{k_f}{k_{f0}} = \left(1 + \frac{\alpha}{\phi_{f0}}\left(\Delta\varepsilon_v + \frac{\Delta p_f}{K_f} - \varepsilon_L \frac{p_m}{P_L + p_m}\right)\right)^3 \tag{8}$$

where $\Delta\varepsilon_v$ is the volumetric strain; ε_L is the Langmuir volumetric strain constant; Δp_f is the change in fracture gas pressure (Pa); K_f is the bulk modulus of the fracture system (Pa). The parameters in the equation can be obtained through experimental data fitting.

3.2. Solid Deformation Control Equation for Coal

The geometric equation describing the deformation of the coal matrix and fractures can be mathematically expressed using the principles of continuum mechanics and rock mechanics. For a dual-porosity coal seam, the relationship between strain and displacement for the coal matrix is governed by the classical Cauchy strain tensor:

$$\varepsilon_{ij} = \frac{1}{2}(\mu_{i,j} + \mu_{j,i}) \tag{9}$$

where ε_{ij} is the strain tensor component; μ_i is the displacement component (m); and i, j are spatial coordinates. Neglecting the influence of inertial forces, the mechanical equilibrium equation governing the deformation behavior of the coal matrix and fractures can be expressed using the principle of stress equilibrium. For a representative elementary volume (REV) of the coal seam, the equation is given by:

$$\sigma_{ij,i} + f_j = 0 \tag{10}$$

where σ_{ij} is the stress tensor component, and f_j is the body force component (N/m^3). This set of equations describes the mechanical equilibrium of the coal mass, accounting for the interactions between solid stress and fluid pressure in both the matrix and fractures. It is assumed that adsorption-induced strain only affects volumetric strain, meaning its components are identical in all three directions. Based on the elastic theory of porous media, the constitutive equation for coal incorporating adsorption effects is expressed as:

$$\varepsilon_{ij} = \frac{1}{2G}\sigma_{ij} - \left(\frac{1}{6G} - \frac{1}{9K}\right)\sigma_{kk}\delta_{ij} + \frac{\alpha}{3K}p_m\delta_{ij} + \frac{\alpha}{3K}p_f\delta_{ij} + \frac{\varepsilon_s}{3}\delta_{ij} \quad (11)$$

where G is the shear modulus of coal (Pa); K is the bulk modulus of coal (Pa); and ε_s is the adsorption strain.

4. Gas Migration Modeling in Ultra-Long Directional Boreholes

4.1. Theoretical Model Validation

The No. 8 coal seam in the Baode Mine exhibits a high proportion of free gas, rapid decay of extraction concentration, and a short effective pre-drainage period. Consequently, achieving target drainage standards requires a relatively long period of time. The mining area is vast, and the working face length exceeds 3000 m, resulting in low efficiency of conventional boreholes and an imbalance among extraction, excavation, and mining. To effectively address these issues, ensure safe production, and maintain operational continuity, this study investigates the gas extraction performance of ultra-long directional boreholes. The research aims to establish a theoretical foundation for large-scale advance gas control underground and to develop a comprehensive gas control technology system for high-gas mines [29,30].

The second mining panel of the No. 8 coal seam extends approximately 3350 m along strike and 2400 m along dip, covering an area of 7.93×10^6 m^2. The mining elevation ranges from +490 m to +680 m. The coal reserves total approximately 8.98×10^7 t, with recoverable reserves of 4.449×10^7 t. The gas content per ton of coal is estimated to be 4.87–8.96 m^3/t for entire panel area, averaging 6.9 m^3/t, corresponding to a gas reserve of approximately 6.2×10^8 m^3.

An advanced composite directional drilling technology was developed by integrating ultra-long directional borehole sliding drilling with drag reduction techniques and a composite trajectory control method. This technology was applied to working face 81209, where ultra-long directional boreholes were deployed along the coal seam. The main borehole reached a depth of 2570 m, with a total drilling length of 3164 m per borehole. Nine branch holes were drilled; roof probing was performed eight times, and floor probing four times. The coal seam drilling rate was 97%, and borehole diameter was 120 mm. Under normal drilling conditions, the average daily drilling rate exceeded 200 m. The actual drilling trajectory in sectional plan view is illustrated in Figure 3.

The numerical model was established with 3D dimensions of 2600 m × 20 m × 6 m, closely matching actual conditions. Roller support constraints were applied at the model bottom and the lateral boundaries, while the overburden rock initial stress was applied at the model top boundary. The mesh consisted of 14,146 quadrilateral elements. For the simulation of methane flow, a drainage pressure of atmospheric pressure at the boundaries of the boreholes in coal was applied, and the remaining boundaries were set as no-flow boundaries. The initial coal seam pressure is 1.2 MPa, and the borehole diameter measures 120 mm. Note that the permeability heterogeneity of the coal body has not been taken into account due to the insignificant permeability heterogeneity in this study area. Physical parameters used in the model were derived from onsite conditions and laboratory tests, as listed in Table 1. The model parameters were derived from experimental test. Langmuir

isotherm parameters were obtained from high-pressure methane sorption experiments. All other parameters were adopted from well-cited studies on analogous coal seams [22].

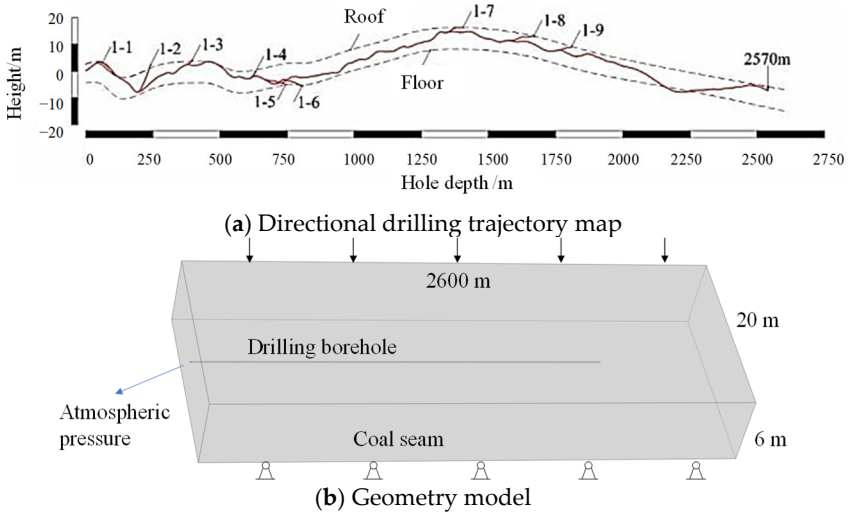

Figure 3. Distribution of drilling boreholes within coal seam.

Table 1. Solution parameters of the numerical model.

Parameter Name	Value	Parameter Name	Value
Shear Modulus of coal, G (MPa)	380	Langmuir pressure constant, P_L (MPa)	2.48
Bulk Modulus of coal matrix, K (MPa)	1143	Langmuir volume constant, V_L (m^3/kg)	0.035
Langmuir volumetric strain, ε_L	0.014	Initial porosity of matrix, ϕ_m (%)	2
Diffusion coefficient of matrix micropores, D (m^2/s)	2.2×10^{-7}	Initial porosity of fractures, ϕ_f (%)	1.5

By inputting the coal's mathematical formulation (Equations (2)–(11)) and physical parameters into COMSOL V6.0 software, the simulated gas extraction rates were compared with field-measured gas flow data to validate the model's accuracy. To improve data reliability, multiple measurements of actual gas extraction rates were averaged. The comparison between simulated and measured gas extraction rates is shown in Figure 4. The blue scatter points represent field-measured gas flow rates, while the orange data points represent the simulation results. It can be observed that, under gas extraction, the borehole gas flow rate gradually increases within the first 10 days, followed by a slow decay trend. The overall simulated gas extraction rates show consistency with the field measurements. Therefore, the coupled model comprising dual-porosity effects of matrix and fracture permeability accurately reflects the actual field conditions.

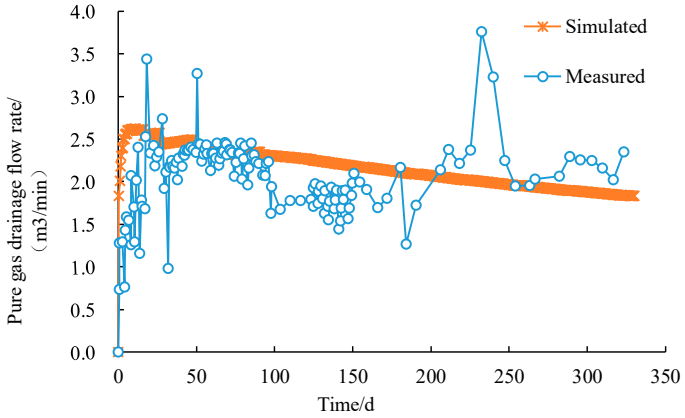

Figure 4. Comparison of field data and simulation results for gas drainage flow rate.

4.2. Influence of Borehole Depth on Gas Extraction

At the beginning drilling and extraction, the variation in pure gas extraction flow rates was monitored in real time and compared with model predictions as the drilling distance increases in Figure 5. The blue curves represent field-measured gas flow rates at various drilling depths, while the orange curves denote simulation results. The total borehole gas flow exhibits a linear increasing trend with drilling depth. The larger the coverage area of the boreholes, the greater the instantaneous extraction flow rate. When the borehole depth is less than 1300 m, the flow rate increases slowly; between 1300 m and 2000 m, the growth rate significantly accelerates; beyond 2000 m, the extraction flow rate tends to stabilize. This indicates a nonlinear relationship between gas extraction flow rate and borehole depth. As the borehole extends deeper into the coal seam, the gas pressure drop zone expands, allowing more high-pressure gas to participate in desorption and migration. Consequently, the gas extraction range increases with borehole depth, resulting in higher extraction flow rates. However, once the borehole depth exceeds a critical threshold, coal wall resistance inside the borehole reduces the negative pressure. A dynamic equilibrium forms between the positive pressure zone at the borehole bottom and the negative pressure extraction zone, limiting the further expansion of the pressure drop zone. Thus, the marginal contribution of increased borehole depth to extraction flow approaches zero, preventing continuous growth in gas extraction flow.

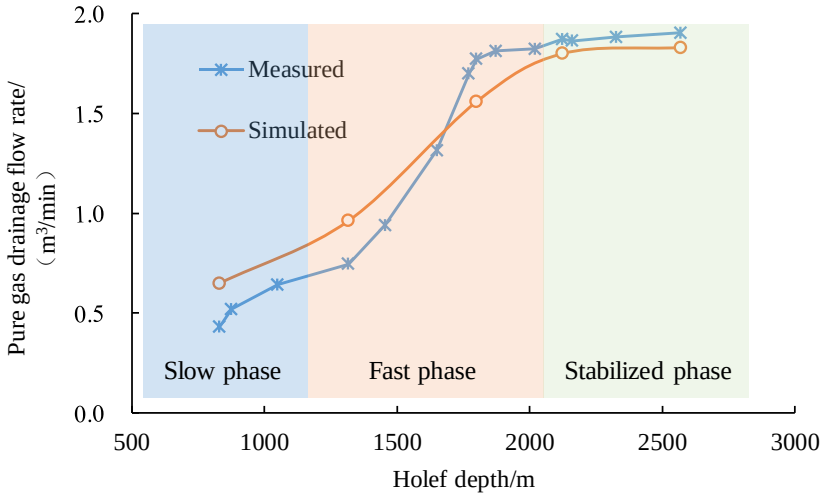

Figure 5. Correlation curve of borehole depth vs. gas drainage flow rate.

During gas extraction, coal seam permeability is jointly controlled by gas pressure and effective stress coupling. As extraction proceeds, the reduction in pore pressure leads to a significant increase in effective stress. This stress increment, applied to the coal skeleton based on effective stress principles, induces compressive deformation of the fracture system, thereby reducing permeability. Conversely, gas desorption from the matrix due to pressure decrease induces matrix shrinkage, which enlarges fracture flow space and thus increases permeability. Under the combined action of these two mechanisms, permeability distribution varies across regions, as shown in Figure 6.

Permeability increases immensely near the borehole inlet in shallow-depth coal regions, where a significant gas pressure drop is observed. Here, permeability can increase by up to 3.5 times within 10 m. It indicates that gas desorption-induced shrinkage has a dominant effect on permeability evolution. In contrast, with increasing borehole depth, the gas pressure drops and desorption range decreases. It consequently weakens the permeability improvement. This trend culminates at depths beyond 1500 m depth, where minimal permeability alteration indicates poor extraction efficiency.

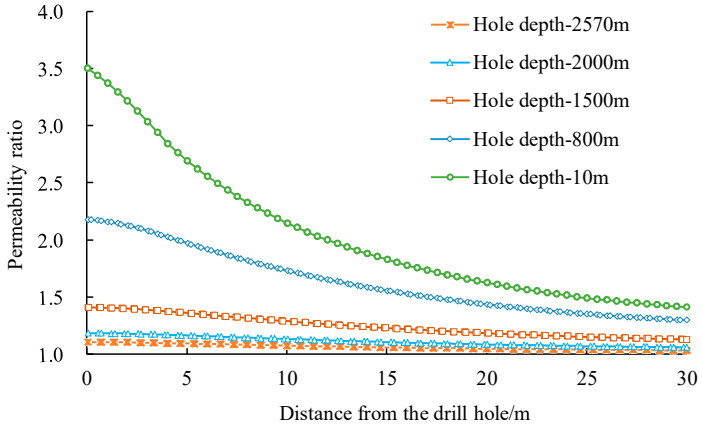

Figure 6. Coal seam permeability ratio vs. borehole depth.

The gas content distribution during coal seam extraction exhibits significant heterogeneity, as illustrated in Figure 7. In shallow-depth regions near the borehole, gas pressure decreases substantially, leading to a marked decline in gas content. Gas content gradually approaches the original level with increasing distance from the borehole. Beyond 2000 m, the decline in gas content is minimal; most areas still exceed 8 m^3/t, indicating the potential risk of gas outburst. The results demonstrate that gas extraction impact at greater depths is significantly reduced.

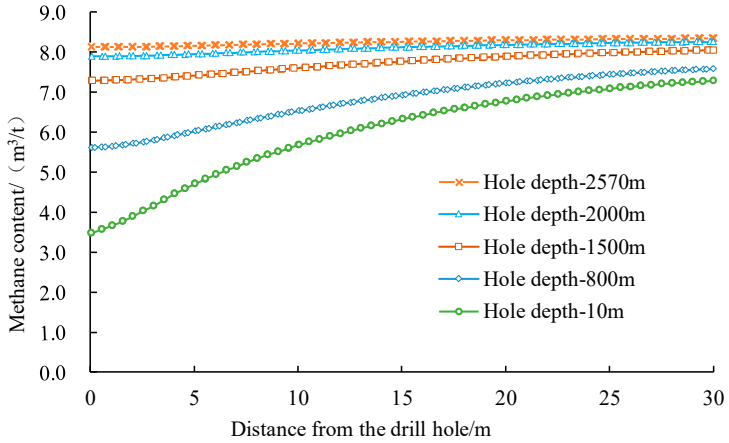

Figure 7. Gas content distribution at different depth of drainage borehole.

5. Conclusions

This study investigated the dynamic evolution of dual-scale pore permeability in the No. 8 coal seam of the Baode mining area, Shanxi Province, during ultra-long directional borehole CBM drainage by integrating laboratory experiments with COMSOL numerical simulations. The main conclusions are as follows:

(1) The permeability difference between matrix and fracture was found to be smaller in low-rank coal under varying stress and pore pressure conditions. This phenomenon attributed to its larger pore structure. Both matrix and fracture permeability decrease gradually with increasing effective stress, indicating a relatively low stress sensitivity of the tested specimens.

(2) Model predicted real-time gas flow rates at various drilling depths are consistent with the field-measured data. The total borehole gas flow exhibits a linear increasing trend with drilling depth. When the borehole depth is less than 1300 m, the flow rate increases slowly; between 1300 m and 2000 m, the growth rate significantly accelerates; beyond 2000 m, the extraction flow rate tends to stabilize.

(3) A reduction in pore pressure increases effective stress, compressing fractures and reducing permeability, whereas gas desorption induces matrix shrinkage, enlarging fracture apertures and enhancing permeability. These mechanisms interact dynamically: pore pressure effects dominate within the first 10 days of drainage, while gas desorption becomes the primary contributor in later stages. In the shallow borehole section (within 10 m of the collar), permeability increased by up to 3.5 times its initial value. At depths exceeding 1500 m, permeability variation was minimal, indicating a limited effectiveness for gas drainage.

(4) Field measurements and simulation results show that in shallow sections (<1500 m), a broad pressure drop zone and sufficient desorption lead to significant permeability enhancement and a rapid increase in drainage flow. In deep sections (>2000 m), limited pressure drops propagation and borehole resistance effects slow permeability growth, stabilize drainage rates, and leave gas content above 8 m^3/t, indicating a pronounced decline in deep drainage efficiency.

Author Contributions: Conceptualization, M.W.; methodology, S.H.; software, Y.L. and S.H. All authors have read and agreed to the published version of the manuscript.

Funding: This work was supported by National Natural Science Foundation of China (U24B2044). These sources of support are gratefully acknowledged.

Institutional Review Board Statement: Not applicable.

Informed Consent Statement: Not applicable.

Data Availability Statement: The original contributions presented in the study are included in the article, further inquiries can be directed to the corresponding author.

Acknowledgments: We appreciate the detailed suggestions and constructive comments from the editor and the anonymous reviewers.

Conflicts of Interest: Author Shuaiyin He was employed by the company CHN Shendong Coal Group Co., Ltd. The remaining authors declare that the research was conducted in the absence of any commercial or financial relationships that could be construed as a potential conflict of interest.

References

1. Liu, D.; Jia, Q.; Cai, Y. Research progress on coalbed methane reservoir geology and characterization technology in China. *Coal Sci. Technol.* **2022**, *50*, 196–203.
2. Wei, M.; Liu, J.; Elsworth, D. Influence of gas adsorption induced non-uniform deformation on the evolution of coal permeability. *Int. J. Rock Mech. Min. Sci.* **2019**, *114*, 71–78. [CrossRef]
3. Wei, J.; Li, B.; Wang, K. Influencing factors on permeability of loaded gas-bearing coal mass. *J. Min. Saf. Eng.* **2014**, *31*, 322–327.
4. Harpalani, S.; Chen, G. Estimation of changes in fracture porosity of coal with gas emission. *Fuel* **1995**, *74*, 1491–1498. [CrossRef]
5. Wang, K.; Wang, L.; Du, F. Evolutionary mechanism of permeability of coal-rock combination considering interface effect: Model development and analysis. *Energy* **2023**, *284*, 129305. [CrossRef]
6. Zhao, C.; Cheng, Y.; Li, W.; Wang, L.; Lu, Z.; Wang, H. A theoretical investigation of coal fracture evolution with hydrostatic pressure and its validation by CT. *Nat. Resour. Res.* **2024**, *33*, 2237–2260. [CrossRef]
7. Jasinge, D.; Ranjith, P.; Choi, S. Effects of effective stress changes on permeability of latrobe valley brown coal. *Fuel* **2011**, *90*, 1292–1300. [CrossRef]
8. Wang, C.; Wang, C.; Tao, Z. Structure deformation of coal induced by gas migration-A case of injecting helium gas into intact coal. *Rock Soil Mech.* **2015**, *36*, 3439–3446.
9. Li, B.; Li, J.; Yang, K. Evolution law of coal permeability based on comprehensive effect of pore pressure and water. *J. China Univ. Min. Technol.* **2020**, *49*, 44–53.
10. Lu, R.; Li, S.; Xue, J. Experimental study on coal seepage characteristics and stress sensitivity. *Saf. Coal Mines* **2022**, *53*, 23–30.
11. Long, Q.; Zhao, X.; Mu, J. Experimental Study on Influence of Pore Gas Pressure upon Gas Permeability of Coal Seam. *Min. Saf. Environ. Prot.* **2008**, *35*, 10–12.

12. Tang, J.; Pan, Y.; Li, C. Experimental study of desorption and seepage of coalbed methane under solid-fluid coupling. *J. China Univ. Min. Technol.* **2006**, *35*, 274–278.
13. Peng, S.; Xu, J.; Yi, G. Experimental analysis of matrix shrinkage's influence on mechanical permeability of gas-filled coal. *J. Chongqing Univ.* **2012**, *35*, 109–114.
14. Zhu, Z.; Feng, T.; Xie, D. Seepage property of coal containing gas under different paths in laboratory. *J. Min. Saf. Eng.* **2012**, *29*, 570–574.
15. Lin, J.; Ren, T.; Wang, G.; Booth, P.; Nemcik, J. Experimental investigation of N2 injection to enhance gas drainage in CO2-rich low permeable seam. *Fuel* **2018**, *215*, 665–674. [CrossRef]
16. Meng, Y.; Wang, J.Y.; Li, Z.; Zhang, J. An improved productivity model in coal reservoir and its application during coalbed methane production. *J. Nat. Gas Sci. Eng.* **2018**, *49*, 342–351. [CrossRef]
17. Pan, Z.; Connell, L.D. Modelling permeability for coal reservoirs: A review of analytical models and testing data. *Int. J. Coal Geol.* **2012**, *92*, 1–44. [CrossRef]
18. Liu, Z.; Cheng, Y.; Liu, Q.; Jiang, J.; Li, W.; Zhang, K. Numerical assessment of CMM drainage in the remote unloaded coal body: Insights of geostress-relief gas migration and coal permeability. *J. Nat. Gas Sci. Eng.* **2017**, *45*, 487–501. [CrossRef]
19. Li, R.; Wang, S.W.; Chao, W.W.; Wang, J.C.; Lyu, S.F. Analysis of the transfer modes and dynamic characteristics of reservoir pressure during coalbed methane production. *Int. J. Rock Mech. Min. Sci.* **2016**, *87*, 129–138. [CrossRef]
20. Wei, M.; Huangfu, H.; Lu, C. Experimental measurement method of matrix and fracture permeability of coal and rock mass. *J. China Univ. Min. Technol.* **2025**, *54*, 413–422.
21. Liu, J.; Chen, Z.; Elsworth, D. Evaluation of stress-controlled coal swelling processes. *Int. J. Coal Geol.* **2010**, *83*, 446–455. [CrossRef]
22. Wu, Y.; Liu, J.; Elsworth, D. Dual poroelastic response of a coal seam to CO2 injection. *Int. J. Greenh. Gas Control* **2010**, *4*, 668–678. [CrossRef]
23. Wei, M.; Liu, J.; Elsworth, D. Impact of equilibration time lag between matrix and fractures on the evolution of coal permeability. *Fuel* **2021**, *290*, 120029. [CrossRef]
24. Robertson, E.P.; Christiansen, R.L. Modeling permeability in coal using sorption-induced strain data. In Proceedings of the 2005 SPE Annual Technical Conference and Exhibition, Dallas, TX, USA, 9–12 October 2005.
25. Shi, J.; Durucan, S. A model for changes in coalbed permeability during primary and enhanced methane recovery. *SPE Reserv. Eval. Eng.* **2005**, *8*, 291–299. [CrossRef]
26. Wang, W.; Li, W.; Wang, L. Analysis of coal permeability model set and prediction effect based on cubic law and meso-scale deformation law. *J. China Coal Soc.* **2025**, 1–21.
27. Connell, L.D.; Mazumder, S.; Sander, R. Laboratory characterization of coal matrix shrinkage, cleat compressibility and the geomechanical properties determining reservoir permeability. *Fuel* **2016**, *165*, 499–512. [CrossRef]
28. Lu, S.; Cheng, Y.; Li, W. Model development and analysis of the evolution of coal permeability under different boundary conditions. *J. Nat. Gas Sci. Eng.* **2016**, *31*, 129–138. [CrossRef]
29. Li, R.; Guo, M. Long distance directional drilling technology in Shendong Mining Area. *Coal Eng.* **2024**, *56*, 53–58.
30. Liu, Z.; Chen, D.; Sun, B. Gas control technology in super large area of high gassy mine. *Coal Sci. Technol.* **2021**, *49*, 120–126.

Disclaimer/Publisher's Note: The statements, opinions and data contained in all publications are solely those of the individual author(s) and contributor(s) and not of MDPI and/or the editor(s). MDPI and/or the editor(s) disclaim responsibility for any injury to people or property resulting from any ideas, methods, instructions or products referred to in the content.